JOURNAL OF COMPUTATIONAL PHYSICS 36, 281–303 (1980)

Use of Artificial Viscosity in Multidimensional Fluid Dynamic Calculations*,†

MARK L. WILKINS

Lawrence Livermore Laboratory, University of California, Livermore, California 95660

Received January 5, 1977; revised July 18, 1979

The von Neumann–Richtmyer concept of artificial viscosity that is used in calculating the propagation of shocks was formulated in one space-dimension. A generalization of the method for two and for three space-dimensions is presented here. The basic objectives were to find the one-dimensional equivalent of shock compression that avoided geometric convergence effects and to determine a characteristic grid length. A description is given of a linear viscosity for damping the spurious oscillations that arise when the quadratic von Neumann–Richtmyer artificial viscosity is used. The linear viscosity minimizes the smearing of the shock front. Unwanted distortions that can occur in multidimensional grids are discussed. Results in two and three dimensions are given for the Navier–Stokes-type viscosity developed to damp these distortions.

I. INTRODUCTION

The concept of artificial viscosity, first introduced in 1950 by von Neumann and Richtmyer [1], has permitted the development of numerical methods for solving the equations of fluid and solid mechanics in one, two, and three space-dimensions and in time. The original formulation of the artificial viscosity q was proposed for calculating the propagation of shocks in an inviscid fluid in one space-dimension. The usual form of the von Neumann q is

$$q_1 = c_0^2 \rho (\Delta x)^2 \left(\frac{\partial \dot{x}}{\partial x}\right)^2, \tag{1}$$

* This work was performed under the auspices of the U.S. Department of Energy by Lawrence Livermore Laboratory under Contract W-7405-Eng-48.

† This report was prepared as an account of work sponsored by the United States Government. Neither the United States nor the United States Department of Energy, nor any of their employees, nor any of their contractors, subcontractors, or their employees, makes any warranty, express or implied, or assumes any legal liability or responsibility for the accuracy, completeness or usefulness of any information, apparatus, product or process disclosed, or represents that its use would not infringe privately-owned rights.

[1] Notation: The artificial viscosities discussed here apply to the equations of fluid and solid mechanics formulated in Lagrange coordinates where the grid moves with the material. A convenient notation is to use a dot over a parameter to designate a time derivative along the particle path. Thus $\dot{x}$, $\dot{y}$, $\dot{z}$ will designate the velocity for a particle at position x, y, z.

0021-9991/80/090281–23$02.00/0

where $q_1 = 0$ for $\partial\dot{x}/\partial x \geqslant 0$, x is the coordinate[1] in the direction of motion, Δx is the grid spacing, ρ is the density, and c_0 is a constant ≈ 2.

Equation (1) can be considered a diffusion equation with a diffusion coefficient [2] α_1 :

$$\alpha_1 = c_0^2 \rho (\Delta x)^2 \left| \frac{\partial \dot{x}}{\partial x} \right|. \tag{2}$$

The diffusion coefficient is scaled to the grid spacing of the problem. A real viscosity coefficient would be independent of the calculational grid; here the function of q is not to represent real viscosity but, rather, to connect over the minimum distance an inviscid state ahead of a shock with that behind the shock. The constant c_0 in Eq. (2) determines the number of grid spacings over which the shock front will spread. The gradient term in Eq. (2) assures that the dissipation occurs in the region of the shock layer. The desired result is to spread the shock over the minimum number of grid spacings while damping the oscillations behind the front caused by the numerical method itself. The von Neumann q of Eq. (1), with a constant c_0 of the order of 2, will spread a shock front over approximately three to five zones. Attempts to reduce the number of zones in the shock front caused overshoots that were slowly damped behind the shock front.

In 1955, Landshoff [3] introduced a q term that was linear in the velocity gradient:

$$q_2 = c_L \rho \, \Delta x a \left| \frac{\partial \dot{x}}{\partial x} \right|, \tag{3}$$

where $q_2 = 0$ for $\partial\dot{x}/\partial x \geqslant 0$, c_L is a constant ≈ 1, and a is the local sound speed.

The Landshoff q of Eq. (3) gives an initial overshoot larger than the Von Neumann q of Eq. (1) but also provides faster damping. The effective diffusion coefficient of the linear viscosity q_2 is

$$\alpha_2 = c_L \rho \Delta x a. \tag{4}$$

Dissipation occurs over a larger distance for the linear viscosity q_2 than for q_1. For shocks propagating in solids, where sound speeds exist even at zero pressure, the effect of the linear q_2 is to diffuse the shock front over an increasing number of zones as the shock propagates. Landshoff recommended a linear combination of the quadratic and linear q to obtain the best features of both:

$$q = q_1 + q_2 . \tag{5}$$

II. Shock-Wave Calculations in One Dimension

A. *Hugoniot Relations*

The artificial viscosity satisfies the Hugoniot relations that connect the state ahead of a shock, traveling with a velocity S, with the state behind. Consider a

shock process in which the state ahead of a shock, traveling at velocity S, is denoted by parameters with subscript 0 and the state behind by parameters with subscript 1:

$$S = \frac{(U_1 - U_0)\,\rho_1}{\rho_1 - \rho_0}, \tag{6}$$

$$P_1 - P_0 = \rho_0 S(U_1 - U_0), \tag{7}$$

$$E_1 - E_0 = \frac{P_1 + P_0}{2}\left(\frac{1}{\rho_0} - \frac{1}{\rho_1}\right), \tag{8}$$

and

$$P = P(E, \rho), \tag{9}$$

where U = particle velocity, P = pressure, and E = specific internal energy. The three Hugoniot relations, Eqs. (6) to (8), and the equation of state (9), provide four equations with five unknowns.

Kuropatenko [4–6] used the above equations directly to obtain a viscosity term for a numerical solution to the equations of fluid dynamics in one space-dimension and time. In the Kuropatenko method for a given calculational zone, the state ahead of the shock is given by the zone parameters at time index n and the state behind by parameters at time index $n + 1$. The change in particle velocity ΔU is the velocity difference across the zone. It is provided by the finite-difference equations of the equations of motion in one space-dimension. With ΔU given, Eqs. (6) through (9) can be solved to determine a new pressure.

The Kuropatenko method can be examined by considering the equation of state of a perfect gas,

$$P = (\gamma - 1)\,\rho E. \tag{10}$$

The system of Eqs. (6), (7), (8), and (10) can be solved explicitly for the pressure P_1 behind the shock:

$$P_1 = P_0 + \frac{\gamma + 1}{4}\rho_0(\Delta U)^2 + \rho_0 |\Delta U| \left[\left(\frac{\gamma + 1}{4}\right)^2 (\Delta U)^2 + a_0^2\right]^{1/2}. \tag{11}$$

Here, ΔU is the change in particle velocity across the shock front and a_0 is the local sound speed ahead of the shock and is equal to $(\gamma P_0/\rho_0)^{1/2}$.

Equation (11) was derived by Hugoniot in 1889 [7, 8]. P_1 is the sum of the pressure ahead of the shock and of two terms with the form of a linear and quadratic vjscosity. As pointed out by Kuropatenko, in the limit of $(\Delta U)^2$ very much larger than a_0^2, the viscosity has the form

$$q = \frac{\gamma + 1}{2}\rho(\Delta U)^2, \tag{12}$$

while in the limit $(\Delta U)^2$ very much smaller than a_0^2, the viscosity has a linear form

$$q = \rho a \mid \Delta U \mid . \tag{13}$$

We find that the particular combination of linear and quadratic viscosity used in Eq. (11) does not seem to be important. The linear and quadratic terms can be collected in the same form as the Landshoff q in Eq. (5). Thus, for a perfect gas equation of state, an artificial viscosity that gives results similar to the Kuropatenko method is

$$q = \left(\frac{\gamma + 1}{2}\right) \rho(\Delta U)^2 + a\rho \mid \Delta U \mid, \tag{14}$$

where $a = (\gamma P/\rho)^{1/2}$, and $q = 0$ for $\Delta U \geqslant 0$.

Figure 1 compares the von Neumann q of Eq. (1) and the q of Eq. (14) for a strong shock in perfect gas, $\gamma = 1.4$. A constant, 10-kbar boundary pressure was applied at

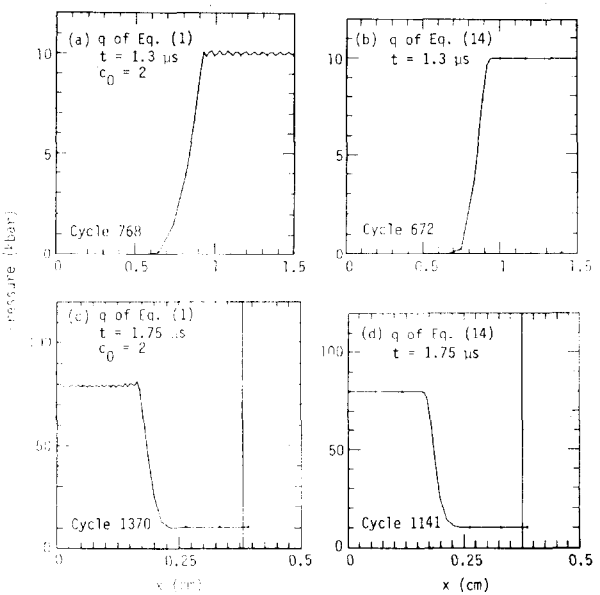

FIG. 1. Comparison of Eqs. (1) and (14) for calculation of a shock in a perfect gas ($\gamma = 1.4$, $\rho_0 = 12 \times 10^{-4}$ g/cm^3). Original grid: length 5 cm, 10 zones/cm; fixed boundary at $x = 0$; right-hand boundary, constant pressure $P = 10$ kbar.

the right-hand side of the grid. The shock proceeds from right to left and reflects from the fixed boundary at $x = 0$. For a perfect gas, the ratio of the reflected shock pressure P_r to the incident shock pressure P_i is $P_r/P_i = 3\gamma - 1/\gamma - 1 = 8$ [7, 8]. Figure 1b shows that an incident shock $P_i = 10$ kbar is moving to the left, and in Fig. 1d the

correct reflected shock pressure $P_r = 80$ kbar has been reached with no numerical overshoots The calculation was performed with 10 zones/cm.

Table I shows a portion of the computer output at $t = 1.2\,\mu$sec but with 30 zones/cm. A constant pressure, $P = 10^{-2}$ Mbar, was applied to the outside boundary of Lagrange zone $J = 151$ (not shown in the table). The shock front is located at the maximum value of the artificial viscosity q. In Table I, this maximum is at $J = 37$, corresponding to an Eulerian position halfway between the positions of $J = 37$ and $J = 38$. The shock front is spread over approximately three zones.

The Hugoniot equations [7, 8] for a 10^{-2}-Mbar (10-kbar) shock in a perfect $\gamma = 1.4$ gas with initial particle velocity $U^0 = 0$, initial pressure $P^0 = 0$, initial energy $E^0 = 0$, and initial density $\rho^0 = 12 \times 10^{-4}$g/cc give:

$$\eta = \frac{\rho}{\rho^0} = \frac{\gamma + 1}{\gamma - 1} = 6, \tag{15}$$

$$\rho^0(\Delta U)^2 = \Delta P(1 - 1/\eta), \tag{16}$$

$$\Delta U = \left(\frac{10^{-2}(5/6)}{1210^{-4}}\right)^{1/2} = 2.6352 \text{ cm}/\mu \text{ sec},$$

$$\Delta E = \tfrac{1}{2}\rho^0(\Delta U)^2 = 4.166610^{-3}\,(10^{12} \text{ ergs per original volume}). \tag{17}$$

Table I shows that the finite-difference program yields results that agree to the fifth significant figure with the solutions to the Hugoniot equations.

For an equation of state of the form $P = K(1/V - 1)$, where K is the bulk modulus and V the relative volume, Eqs. (6) through (8) can also be solved explicitly for the shock pressure P_1 if the state ahead of shock S is known and the change in particle velocity ΔU is given:

$$P_1 = P_0 + \rho_0 \frac{\Delta U}{2} S = P_0 + \frac{1}{2}\rho_0(\Delta U)^2 + \rho_0(\Delta U)\left[\left(\frac{\Delta U}{2}\right)^2 + a_0^2\right]^{1/2}, \tag{18}$$

where a_0 is the local sound speed $= (K/\rho_0)^{1/2}$

As with the perfect gas example, a linear and quadratic viscosity can be identified. In the limit of $(\Delta U)^2$ larger than a_0^2, the viscosity is

$$q = \rho_0(\Delta U)^2. \tag{19}$$

In the limit of $(\Delta U)^2$ smaller than a_0^2, the viscosity is

$$q = \rho_0 a_0 \Delta U. \tag{20}$$

B. *Oscillations behind the Shock Front*

We find that for stress waves in solids, the artificial viscosity coefficients determined by the Hugoniot relations and the equation of state do not always provide

TABLE I

Numerical Output at $t = 1.2\ \mu$sec for the Region near the Shock Front[a]

TIME	CYCLE	DTO	P-JMAX
1.20057084E+00	1846	6.49460435E-04	1.00000000E-02

J	X	U	P	Q	E	ETA
00104	1.575142E+00	-2.6353E+00	1.00000E-02	0.	4.1670E-03	5.9996E+00
00103	1.569586E+00	-2.6353E+00	1.00000E-02	0.	4.1669E-03	5.9996E+00
00102	1.564031E+00	-2.6353E+00	1.00001E-02	4.66666E-10	4.1669E-03	5.9997E+00
00101	1.558475E+00	-2.6353E+00	1.00001E-02	2.56009E-10	4.1669E-03	5.9997E+00
00100	1.552919E+00	-2.6353E+00	1.00001E-02	5.12700E-10	4.1668E-03	5.9998E+00
00099	1.547363E+00	-2.6353E+00	1.00001E-02	8.20126E-10	4.1668E-03	5.9998E+00
00098	1.541808E+00	-2.6353E+00	1.00001E-02	1.06905E-09	4.1668E-03	5.9999E+00
00097	1.536252E+00	-2.6353E+00	1.00001E-02	1.25104E-09	4.1668E-03	5.9999E+00
00096	1.530696E+00	-2.6353E+00	1.00001E-02	1.33998E-09	4.1668E-03	5.9999E+00
00095	1.525141E+00	-2.6353E+00	1.00001E-02	1.31490E-09	4.1667E-03	6.0000E+00
00094	1.519585E+00	-2.6353E+00	1.00001E-02	1.15726E-09	4.1667E-03	6.0000E+00
00093	1.514030E+00	-2.6353E+00	1.00001E-02	8.45528E-10	4.1667E-03	6.0000E+00
00092	1.508474E+00	-2.6353E+00	1.00001E-02	3.79493E-10	4.1667E-03	6.0000E+00
00091	1.502919E+00	-2.6353E+00	1.00001E-02	0.	4.1667E-03	6.0000E+00
00090	1.497363E+00	-2.6353E+00	1.00001E-02	0.	4.1667E-03	6.0001E+00
00089	1.491808E+00	-2.6353E+00	1.00001E-02	0.	4.1666E-03	6.0001E+00
00088	1.486252E+00	-2.6353E+00	1.00001E-02	0.	4.1666E-03	6.0001E+00
00087	1.480697E+00	-2.6353E+00	1.00001E-02	0.	4.1666E-03	6.0001E+00
00086	1.475141E+00	-2.6353E+00	1.00001E-02	0.	4.1666E-03	6.0001E+00
00085	1.469586E+00	-2.6353E+00	1.00001E-02	0.	4.1666E-03	6.0001E+00
00084	1.464031E+00	-2.6353E+00	1.00001E-02	0.	4.1666E-03	6.0001E+00
00083	1.458475E+00	-2.6353E+00	1.00001E-02	0.	4.1666E-03	6.0002E+00
00082	1.452920E+00	-2.6353E+00	1.00001E-02	0.	4.1666E-03	6.0002E+00
00081	1.447364E+00	-2.6353E+00	1.00001E-02	3.60449E-10	4.1666E-03	6.0002E+00
00080	1.441809E+00	-2.6353E+00	1.00001E-02	1.72689E-10	4.1666E-03	6.0002E+00
00079	1.436254E+00	-2.6353E+00	1.00001E-02	4.66440E-10	4.1666E-03	6.0002E+00
00078	1.430698E+00	-2.6353E+00	1.00001E-02	9.52294E-10	4.1666E-03	6.0002E+00
00077	1.425143E+00	-2.6353E+00	1.00001E-02	1.37691E-09	4.1666E-03	6.0002E+00
00076	1.419588E+00	-2.6353E+00	1.00001E-02	1.63310E-09	4.1665E-03	6.0002E+00
00075	1.414032E+00	-2.6353E+00	1.00001E-02	1.66107E-09	4.1665E-03	6.0002E+00
00074	1.408477E+00	-2.6353E+00	1.00001E-02	1.43720E-09	4.1666E-03	6.0002E+00
00073	1.402922E+00	-2.6353E+00	1.00001E-02	9.69426E-10	4.1665E-03	6.0002E+00
00072	1.397366E+00	-2.6353E+00	1.00001E-02	2.68001E-10	4.1665E-03	6.0003E+00
00071	1.391811E+00	-2.6353E+00	1.00001E-02	0.	4.1665E-03	6.0003E+00
00070	1.386256E+00	-2.6353E+00	1.00001E-02	0.	4.1665E-03	6.0003E+00
00069	1.380700E+00	-2.6353E+00	1.00001E-02	0.	4.1665E-03	6.0003E+00
00068	1.375145E+00	-2.6353E+00	1.00001E-02	0.	4.1665E-03	6.0003E+00
00067	1.369590E+00	-2.6353E+00	1.00001E-02	0.	4.1665E-03	6.0003E+00
00066	1.364034E+00	-2.6353E+00	1.00001E-02	0.	4.1665E-03	6.0003E+00
00065	1.358479E+00	-2.6353E+00	1.00001E-02	0.	4.1665E-03	6.0003E+00
00064	1.352924E+00	-2.6353E+00	1.00001E-02	0.	4.1665E-03	6.0003E+00
00063	1.347369E+00	-2.6353E+00	1.00001E-02	0.	4.1665E-03	6.0003E+00
00062	1.341813E+00	-2.6353E+00	1.00001E-02	0.	4.1665E-03	6.0003E+00
00061	1.336258E+00	-2.6353E+00	1.00001E-02	0.	4.1665E-03	6.0003E+00
00060	1.330703E+00	-2.6353E+00	1.00001E-02	0.	4.1665E-03	6.0003E+00
00059	1.325148E+00	-2.6353E+00	1.00001E-02	0.	4.1665E-03	6.0003E+00
00058	1.319592E+00	-2.6353E+00	1.00001E-02	5.92514E-10	4.1665E-03	6.0003E+00
00057	1.314037E+00	-2.6353E+00	1.00002E-02	8.71760E-10	4.1665E-03	6.0003E+00
00056	1.308482E+00	-2.6353E+00	1.00002E-02	7.75447E-10	4.1665E-03	6.0004E+00
00055	1.302927E+00	-2.6353E+00	1.00002E-02	4.02185E-10	4.1665E-03	6.0004E+00
00054	1.297372E+00	-2.6353E+00	1.00002E-02	0.	4.1665E-03	6.0004E+00
00053	1.291816E+00	-2.6353E+00	1.00002E-02	0.	4.1665E-03	6.0004E+00
00052	1.286261E+00	-2.6353E+00	1.00002E-02	1.28065E-09	4.1665E-03	6.0004E+00
00051	1.280706E+00	-2.6353E+00	1.00002E-02	0.	4.1665E-03	6.0004E+00
00050	1.275151E+00	-2.6353E+00	1.00002E-02	0.	4.1665E-03	6.0004E+00
00049	1.269596E+00	-2.6353E+00	1.00002E-02	1.85173E-09	4.1665E-03	6.0004E+00
00048	1.264040E+00	-2.6353E+00	1.00002E-02	1.81639E-08	4.1665E-03	6.0004E+00
00047	1.258485E+00	-2.6353E+00	1.00002E-02	0.	4.1665E-03	6.0004E+00
00046	1.252930E+00	-2.6353E+00	1.00001E-02	0.	4.1665E-03	6.0004E+00
00045	1.247375E+00	-2.6353E+00	1.00000E-02	1.81981E-07	4.1664E-03	6.0003E+00
00044	1.241820E+00	-2.6352E+00	1.00001E-02	2.34420E-07	4.1664E-03	6.0004E+00
00043	1.236264E+00	-2.6353E+00	1.00002E-02	0.	4.1665E-03	6.0004E+00
00042	1.230709E+00	-2.6353E+00	9.99914E-03	0.	4.1663E-03	6.0000E+00
00041	1.225150E+00	-2.6345E+00	9.99075E-03	7.62955E-06	4.1653E-03	5.9964E+00
00040	1.219562E+00	-2.6270E+00	9.91921E-03	7.50939E-05	4.1568E-03	5.9657E+00
00039	1.213719E+00	-2.5638E+00	9.30963E-03	6.24800E-04	4.0802E-03	5.7042E+00
00038	1.206051E+00	-2.1953E+00	6.17430E-03	3.23187E-03	3.5509E-03	4.3470E+00
00037	1.191638E+00	-1.2525E+00	1.74692E-03	5.21667E-03	1.8883E-03	2.3128E+00
00036	1.165922E+00	-2.2379E-01	1.27930E-04	2.44207E-03	2.4673E-04	1.2962E+00
00035	1.133329E+00	-2.5208E-03	2.59051E-07	7.60112E-05	6.3325E-07	1.0227E+00
00034	1.100000E+00	-1.0573E-07	0.	9.22704E-09	0.	1.0001E+00
00033	1.066667E+00	0.	0.	0.	0.	1.0000E+00
00032	1.033333E+00	0.	0.	0.	0.	1.0000E+00
00031	1.000000E+00	0.	0.	0.	0.	1.0000E+00

[a] For problem given in Fig. 1; q from Eq. (14); 30 zones/cm; J = Lagrange coordinate; x = position (cm); U = particle velocity (cm/μsec); P = pressure (Mbar); Q = artificial viscosity (Mbar); E = internal energy (10^{12} erg per original volume); ETA = compression = current density/reference density.

sufficient damping of numerical oscillations behind the front. This is especially true with problems involving Hooke's Law. Because most students of numerical methods in hydrodynamics are familiar with the Landshoff q, it is convenient to retain this form and to use adjustable constants to provide the required damping. However, in place of the actual sound speed of the material in the linear portion of q, a term proportional to the sound speed for a perfect gas is used for all materials, solid and gaseous:

$$q = c_0^2 \rho (\Delta U)^2 + c_L a \rho \mid \Delta U \mid , \tag{21}$$

where $q = 0$ for $\Delta U \geqslant 0$, $c_0 = 2$, $c_L = 0.8$, ΔU is the difference in particle velocity across the zone, $a = (P/\rho)^{1/2}$, P is the zone pressure, and ρ is the zone density.

This q, with the constants shown, can be used for a wide range of shock pressures and equations of state. The advantage of using the parameter a in the linear portion of the viscosity is that it provides a zero diffusion coefficient for waves propagating

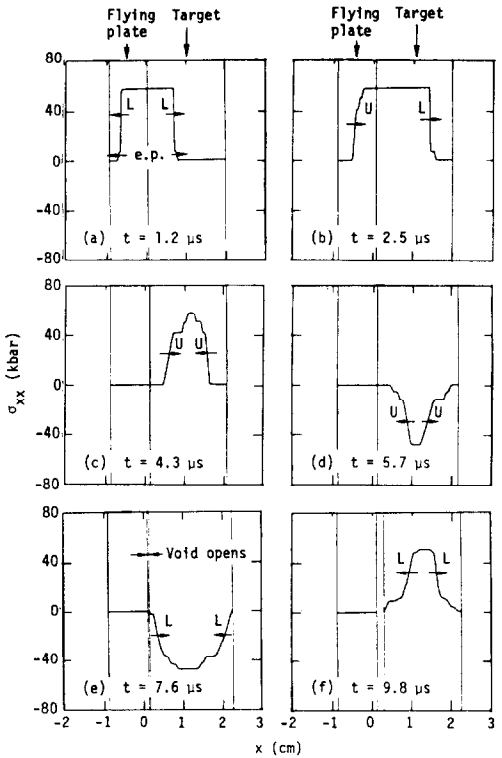

FIG. 2. Calculated stress waves σ_{xx} in an elastic, perfectly plastic material at various times after a flying-plate impact (L = loading wave, e.p. = elastic precursor, U = unloading wave). Impact velocity: 0.07 cm/μsec. Equation of state: pressure $P = 0.73(\eta - 1) + 1.72(\eta - 1)^2 + 0.4(\eta - 1)^3$ Mbar; compression $\eta = \rho/\rho_0$; density $\rho_0 = 2.7$ g/cm^3; shear modulus $\mu = 0.248$ Mbar; flow stress $Y_0 = 0.002976$ Mbar; $\sigma_{xx} = -P + s_{xx}$, where s_{xx} = stress deviator.

in solids at rest. This property helps to minimize the undesirable diffusion associated with a linear viscosity. With the formulation shown, the linear viscosity becomes effective behind the front, where it is needed to damp numerical overshoots.

For specific problems, the shock front can be sharpened by adjusting the constants of Eq. (21). Figure 2 shows the calculated stresses associated with the impact of a flying plate against a target plate. The materials are described by an elastic, perfectly plastic, constitutive relation. The adjusted constants were $c_0 = 1.4$ and $c_L = 0.5$, and the calculation used 100 zones/cm. The structure in the wave profile after it reaches a free surface can be attributed to the fact that the elastic portions of the wave unload faster than the plastic ones. The precursor reflects from the free surface and unloads the elastic-compression portion of the wave. When the modified wave reaches the free surface, the elastic portion becomes tensile, giving a second step to the reflected wave profile.

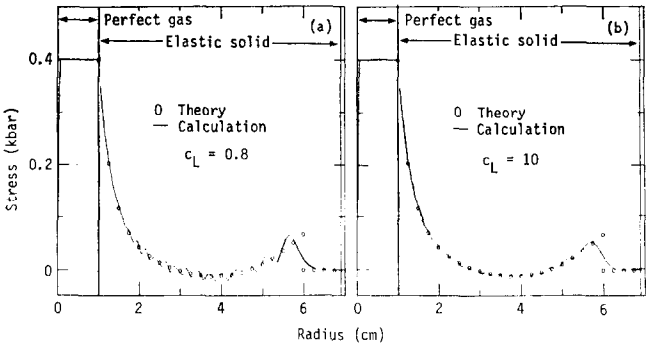

FIG. 3. Comparison of theory and calculation for a spherically diverging wave in a linear elastic solid using Eq. (21) (10 zones/cm; $t = 8.7$ μsec; $c_0 = 2$): (a) $c_L = 0.8$ and (b) $c_L = 10$. Equations of state (perfect gas): $\gamma = 1.4$; density $\rho_0 = 0.8$ g/cm³; initial pressure $P = 0.4$ kbar; initial radius $R = 1$ cm. Equation of state (elastic solid, Hooke's law): bulk modulus $K = 0.5$ Mbar; shear modulus $\mu = 0.3$ Mbar; density $\rho_0 = 2.7$ g/cm³. Figure shows the radial stress positive in compression.

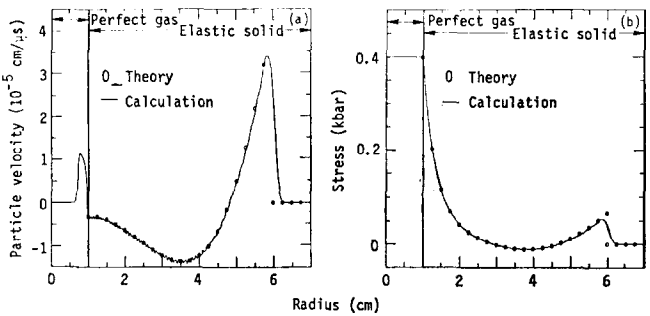

FIG. 4. Comparison of theory and calculation for a spherically diverging wave in a linear elastic solid using Eq. (21) (30 zones/cm; $t = 8.7$ μsec; $c_L = 10$; $c_0 = 2$): (a) particle velocity and (b) stress, shown positive in compression.

That centered difference schemes introduce oscillations into a calculation when a sudden pressure is applied to a boundary is well known. This problem is particularly pronounced for low-level signals propagating in linear-elastic solids (Hooke's Law). Figure 3a shows results of a calculation of a weak spherically diverging wave propagating in a linear elastic solid. The q constants are the same as those given in Eq. (21). In this example, only the linear portion of q is operative, since $(\Delta U)^2 \ll |\Delta U|$. In Fig. 3b, the same problem is calculated with a larger linear viscosity term, $c_L = 10$. Smoother results can be obtained with finer zoning. Figure 4 shows results for the same problem ($c_L = 10$) calculated with three times as many zones. The theoretical results shown in Figs. 3 and 4 were obtained from Ref. [10].

III. Shock-Wave Calculations in Two and Three Dimensions

A. *Strain Rate*

In extending the one-dimensional von Neumann–Richtmyer idea to two and three dimensions, two basic problems must be solved. The first is to obtain an expression for the rate of strain given by the velocity gradient in Eq. (1). The second is to obtain a characteristic grid length. Most researchers use the continuity equation to replace the divergence of the velocity with the rate of change of volume. Actually, this was part of the original artificial viscosity formulation of von Neumann and Richtmyer. A shock process is assumed to occur when the volume of a zone is compressed in the direction of motion; but in two and three space dimensions, the volume of a zone may be compressed because of convergence of flow. To describe a shock, we must know the rate of change of the volume that is caused by one surface overtaking another surface (provided by $\partial \dot{x}/\partial x$ for flow in one space-dimension). This can be obtained by calculating the rate of strain in the direction of acceleration. Equation (22) gives the rate

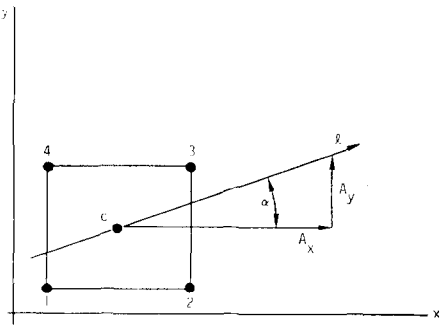

FIG. 5. Scheme for calculating the rate of strain ds/dt of a zone defined by points 1, 2, 3, and 4: l = line in the direction of acceleration; point c = zone center taken from average of coordinates 1 to 4; and A_x and A_y are the x and y components of acceleration obtained by averaging the respective components of the four points.

of change of an element of length divided by that length in the direction of angle α for two space-dimensions [11]:

$$\frac{ds}{dt} = \frac{\partial \dot{x}}{\partial x} \cos^2 \alpha + \frac{\partial \dot{y}}{\partial y} \sin^2 \alpha + \left(\frac{\partial \dot{x}}{\partial y} + \frac{\partial \dot{y}}{\partial x}\right) \cos \alpha \sin \alpha. \tag{22}$$

The derivation of this expression can be found in Ref. [12, Chaps. 1, 2]. When angle α is the direction of acceleration, Eq. (22) provides the two-dimensional analog of the one-dimensional rate of strain $\partial \dot{x}/\partial x$. If A_x and A_y are the x and y components of acceleration of a zone (see Fig. 5), then

$$\cos \alpha = A_x/(A_x^2 + A_y^2)^{1/2},$$
$$\sin \alpha = A_y/(A_x^2 + A_y^2)^{1/2}.$$

The general expression for ds/dt in three space-dimensions [12] is given by

$$\frac{ds}{dt} = \left[\frac{\partial \dot{x}}{\partial x}(A_x)^2 + \frac{\partial \dot{y}}{\partial y}(A_y)^2 + \frac{\partial \dot{z}}{\partial z}(A_z)^2 + \left(\frac{\partial \dot{x}}{\partial y} + \frac{\partial \dot{y}}{\partial x}\right) A_x A_y + \left(\frac{\partial \dot{x}}{\partial z} + \frac{\partial \dot{z}}{\partial x}\right) A_x A_z + \left(\frac{\partial \dot{y}}{\partial z} + \frac{\partial \dot{z}}{\partial y}\right) A_y A_z\right] \cdot \left[\frac{1}{A_x^2 + A_y^2 + A_z^2}\right]. \tag{23}$$

B. *Characteristic Grid Length*

The second basic problem is to obtain a characteristic grid length in a multidimensional grid. Such a quantity is easily obtained for the one-dimensional fluid equations of von Neumann and Richtmyer. In two space-dimensions, the square root of the grid

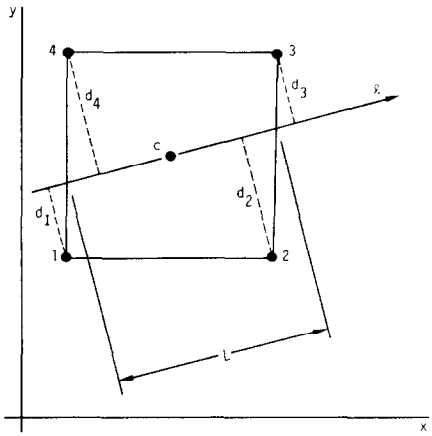

FIG. 6. Scheme for obtaining a characteristic grid length L: l = line through zone center c in direction of acceleration; d_i = perpendicular distance from point i (1, 2, 3, 4) to line l; and $L = 2A/(d_1 + d_2 + d_3 + d_4)$, where A = area of the zone.

area has been used, and in three space-dimensions, the cube root of the volume. None of these methods permits the two- or three-dimensional problem to reduce the one-dimensional results. A serious objection arises if the zones are distorted or if a zone has a large aspect ratio.

Consider a long, thin zone in two dimensions. The zone area can be large and can give a large, effective q coefficient even though the shock is moving in the direction of the smallest length. We can overcome this difficulty by defining a grid length L in the direction of [illegible]

The generalized q is then given as

$$q = c_0^2 \rho L^2 \left(\frac{ds}{dt}\right)^2 + c_L \rho L a \left|\frac{ds}{dt}\right|, \tag{24}$$

where

$$q = 0 \qquad \text{for} \quad \frac{ds}{dt} \geqslant 0,$$

$$L = \frac{2A}{d_1 + d_2 + d_3 + d_4},$$

$$\frac{ds}{dt} = \frac{\partial \dot{x}}{\partial x} \cos^2 \alpha + \frac{\partial \dot{y}}{\partial y} \sin^2 \alpha + \left(\frac{\partial \dot{x}}{\partial y} + \frac{\partial \dot{y}}{\partial x}\right) \cos \alpha \sin \alpha,$$

$$a = (P/\rho)^{1/2},$$

$$c_0 \simeq 2,$$

and

$$c_L \simeq 1.$$

Here, A is the area of a grid defined by four nodes and d is the perpendicular distance from a grid node to a line through the grid center (see Fig. 6). This q has been used for many years in the two-dimensional HEMP program [9] at the Lawrence Livermore Laboratory to solve a large number of problems. The characteristic zone length L can also be used in the time-step control to satisfy the Courant condition, thus permitting a larger time step for motion in the direction of the largest zone length.

The method can be extended into three space-dimensions, although calculating the characteristic grid length L then becomes a cumbersome process. With the q given by Eq. (24), a plane shock in one space-dimension can be exactly duplicated with the one-, two-, and three-dimensional programs.

Figure 7 shows a grid for demonstrating in plane geometry the artificial viscosity described above. A pressure source in the circular region causes a cylindrically divergent shock to propagate through the two-dimensional grid. On any radius, the wave profile should be the same. With the grid set up in this fashion, the wave must traverse the grid at different angles. In the direction of the x and y axes, the shock wave

moves in the direction of the grid. For a radius of 45° from the x or y axis, the shock wave moves diagonally through the grid. Figure 8 shows the wave profiles for these two extreme conditions. For comparison, a calculation in one space-dimension is also shown. The first two profiles closely agree. Some differences are expected because of the finite number of zones in the problem. For zones per unit length, the number in the 45° direction is less by a factor of $\frac{1}{2}^{1/2}$ compared to the number in the direction of the x axis.

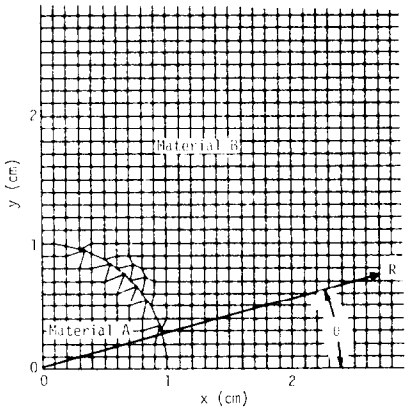

FIG. 7. Two-dimensional grid in plane geometry used for calculating a cylindrically diverging pressure wave. For material A, a perfect gas: $\gamma = 1.4$, $\rho_0 = 0.8$ g/cm³. For material B: $P = 0.73(\eta - 1) + 1.72(\eta - 1)^2 + 0.4(\eta - 1)^3$, $\rho_0 = 2.7$ g/cm³, and $\eta = \rho/\rho_0$.

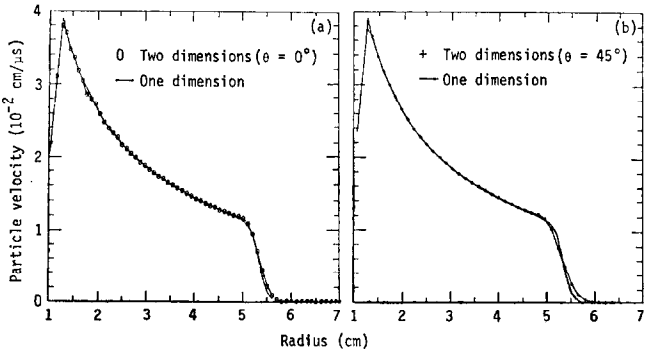

FIG. 8. Comparison of one- and two-dimensional calculations of particle velocity vs radius at $t = 8$ μsec. In the two-dimensional calculations, the grid of Fig. 7 was used. Results are shown for two different values of θ.

Figure 9 illustrates a calculation for a strong shock moving into a region of long, narrow zones [13], the region itself being shown in Fig. 9a. Figure 9b shows results calculated with a characteristic grid length based on the square root of the zone area. Large distortions occur in the regions where the aspect ratio of the zones is very large.

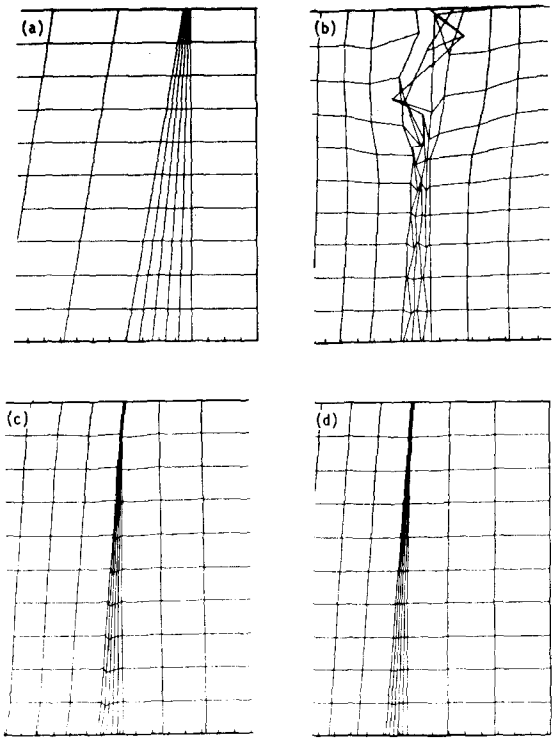

FIG. 9. Calculation of a strong shock in a perfect gas ($\gamma = 3$), with long narrow zones in the center of the grid: (a) grid at $t = 0$; (b) grid after shock has passed from left to right (characteristic grid length L = square root of zone area); (c) same as (b) but with characteristic grid length L given by Eq. (24); (d) same as (c) but with addition of triangle viscosity $C_{NS} = 0.05$.

Figure 9c shows the same calculation using the q discussed above. The shock passes through this region without causing a large perturbation. In Fig. 9d, a grid stabilizing viscosity has been added.

C. *Grid Stabilization*

In addition to the spurious oscillation behind a shock or compression wave in one, two, or three dimensions, a linear instability can occur in two and three dimensions. In two-dimensional problems, a quadrilateral calculational grid is almost always used, because it allows large displacements and deformation to occur without introducing the artificial stiffness typical of triangular zones. Experience with triangular grids for two-dimensional flow and tetrahedral grids for three-dimensional flow shows that these grids not only introduce an artificial stiffness for compressible-flow problems but also introduce asymmetries into the calculation. Results differ depending on the direction of orientation of the triangles or tetrahedrons in a given region discretized by the grid. However, unwanted "hourglass" distortions can occur with quadri-

lateral and cubical grids (see Fig. 9b). For a quadrilateral zone in two space-dimensions, there are eight degrees of freedom, but not all of these lead to distortion. For example, there are two degrees of freedom for translations in the x and y directions and one for rigid rotation; with the elastic–plastic formulation, there are three components of stress that can resist distortion. However, there remain two degrees of freedom with no restorting forces, and these result in hourglass distortions in the two coordinate directions. In three space-dimensions, the problem is more acute, as there

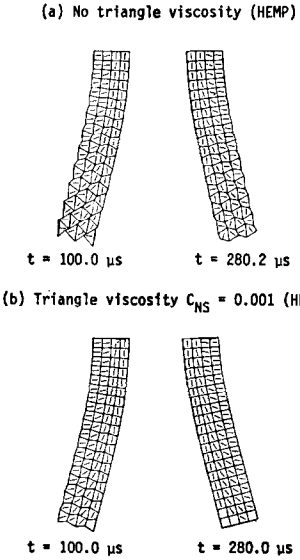

FIG. 10. Comparison of two-dimensional calculations for a vibrating plate (length = 52.5 mm, thickness = 10 mm) clamped at the top edge: (a) without and (b) with triangle viscosity. (Displacements are multiplied by 10). The short lines in the grid show the direction of the maximum principal stress. Elastic constants: bulk modulus K = 1.88 Mbar; shear modulus μ = 0.214 Mbar; density ρ_0 = 7.72 g/cm³.

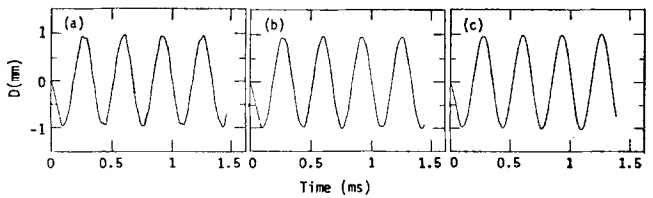

FIG. 11. Effect of triangle viscosity C_{NS} on displacement D as a function of time for the center-point on bottom edge of plate shown in Fig. 10: (a) C_{NS} = 0; (b) C_{NS} = 0.001; (c) C_{NS} = 0.005.

are 24 degrees of freedom associated with cubical zones. Three translation directions and three rigid rotations do not contribute to distortion and six components of strain can give stresses that respond to distortion; this leaves 12 degrees of freedom unaccounted for.

Most of the two-dimensional Lagrange codes incorporate methods for overcoming the hourglass distortion. For example, in the TENSOR code [14] a viscosity is developed based on the rotation of one side of a zone relative to the opposite side. The method used for the two-dimensional HEMP [9] program is a Navier–Stokes tensor artificial viscosity based on triangles (see Appendix A). The three-dimensional analog for the HEMP 3D program is a viscosity based on tetrahedrons (see Appendix B and Ref. [15]).

For a given quadrilateral zone in two dimensions there is a tensor articial viscosity for each of the four nodes that define the zone. Similarly, in three dimensions there will be a tensor artificial viscosity for each of the eight nodes making up a given cubical zone. With these viscosities included in the acceleration equations, no unaccounted distortions to the quadrilateral or cubical grids occur. The artificial viscosities described in Appendixes A and B also can damp motion of interest. They

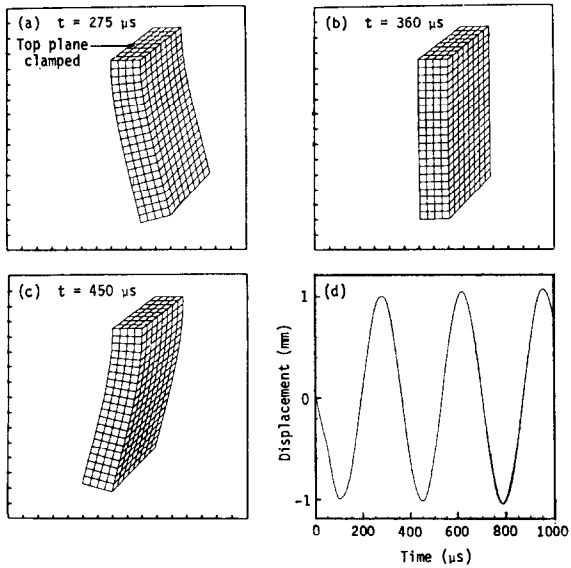

FIG. 12. A HEMP 3D simulation of the motion of a vibrating elastic plate (52.5 × 20 × 10 mm): (a) position of maximum positive displacement; (b) position of maximum kinetic energy; (c) position of maximum negative displacement; (d) displacement history for a point in the geometric center of the bottom plane. Elastic constants: bulk modulus $K = 1.88$ Mbar; shear modulus $\mu = 0.814$Mbar; density $\rho_0 = 7.72\, g/cm^3$. Tetrahedron viscosity: $C_{NS} = 0.01$.

should be used obly for problems that show a tendency toward hourglass distortion. The magnitude of the viscosities can be limited by the viscosity constant C_{NS} (see Appendixes A and B). Static solutions can be obtained with time-dependent calculations by using a large value of the viscosity constant C_{NS} to damp kinetic energy.

Figures 10 and 11 show results in two space-dimensions, and Fig. 12 shows results in three space-dimensions. The energy dissipated by the tensor artificial viscosities

can be evaluated by summing the product of the viscous stresses and the corresponding incremental strains.

Figure 13 shows results for the same spherically diverging one-dimensional calculation given in Fig. 3, but the two-dimensional HEMP program was used here with the grid of Fig. 7 and cylindrical symmetry about the x axis. The q constants of Eq. (24) were $c_L = 10$ and $c_0 = 2$. In addition, a triangle tensor artificial viscosity with coefficient $C_{NS} = 0.02$ was used. Figure 13 shows the particle velocity profiles along the x

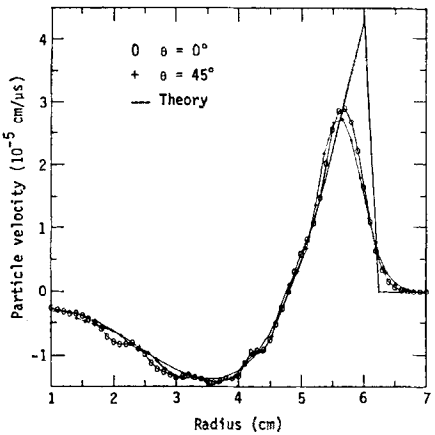

FIG. 13. Calculation of a spherically diverging wave in an elastic solid. The grid shown in Fig. 7 was used with cylindrical symmetry about the x axis. Geometry and material were the same as in Fig. 3: $c_L = 10$; $C_{NS} = 0.02$.

axis (where there are 20 zones/cm) and also along a radius at 45° to the x axis. The number of zones cm in the 45° direction is $20/2^{1/2}$. The agreement with the theoretical calculation is about the same as for results from a one-dimensional calculation. As mentioned earlier, in finite-difference calculations, the propagation of a weak, spherically diverging wave in a linear-elastic solid poses greater difficulties than does wave propagation in nonlinear solids. The purpose of the calculation in Fig. 13 is to show that results comparable to a one-dimensionsl calculation can be obtained with the two-dimensional program, even though the grid was not set up to accommodate the flow.

IV. CONCLUSIONS

For calculating the shock waves in two and three dimensions, a generalized method is presented that reduces to the one-dimensional method of von Neumann and Richtmyer. A linear viscosity that minimizes the diffusion of the shock front is incorporated with the von Neumann–Richtmyer viscosity to damp numerical over shoots occurring behind the shock front. Tensor artificial viscosities that stabilize distortion occurring in two-dimensional quadrilateral and three-dimensional cubical

grids are given. It is desirable to formulate the difference equations with quadrilateral and cubical grids, because these grids can undergo large deformations compared to triangular or tetrahedral grids.

APPENDIX A: TENSOR ARTIFICIAL VISCOSITY FOR STABILIZING A TWO-DIMENSIONAL GRID

A Navier–Stokes viscosity is formulated by using triangles to prevent grid distortion and is referred to as the "triangle q." Figure A.1 shows the grid for calculating the

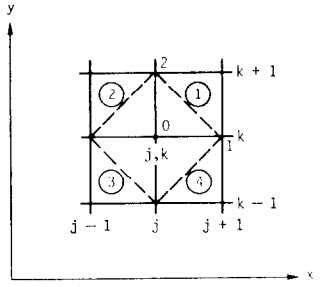

FIG. A.1. Two-dimensional grid for accelerating point (j, k).

acceleration of point (j, k). A triangle q, expressed as a stress deviator, is formulated for each of the triangles in the four zones surrounding point (j, k). For example, the artificial viscosities for zone 1 are given by

$$q_{xx} = 2\mu_1[2/3\dot{\epsilon}_{xx} - 1/3\dot{\epsilon}_{yy}],$$
$$q_{yy} = 2\mu_1[2/3\dot{\epsilon}_{yy} - 1/3\dot{\epsilon}_{xx}],$$
$$q_{xy} = \mu_1\dot{\epsilon}_{xy},$$

where

$$\mu_1 = C_{\mathrm{NS}}(\rho_0/V)A^{1/2};$$
$$A = \text{area of triangle (0, 1, 2,)};$$
$$C_{\mathrm{NS}} = \text{constant} \approx 10^{-3};$$
$$\rho_0 = \text{zone reference density};$$

and

$$V = \text{zone relative volume}.$$

Velocity strains for triangle (0, 1, 2) are:

$$\dot{\epsilon}_{xx} = \frac{\partial \dot{x}}{\partial x} = -\frac{1}{A}\{\dot{x}_{01}(y_0 - y_1) + \dot{x}_{12}(y_1 - y_2) + \dot{x}_{20}(y_2 - y_0)\},$$

$$\dot{\epsilon}_{yy} = \frac{\partial \dot{y}}{\partial y} = +\frac{1}{A}\{\dot{y}_{01}(x_0 - x_1) + \dot{y}_{12}(x_1 - x_2) + \dot{y}_{20}(x_2 - x_0)\},$$

$$\dot{\epsilon}_{xy} = \frac{\partial \dot{y}}{\partial x} + \frac{\partial \dot{x}}{\partial y} = -\frac{1}{A}\{\dot{y}_{01}(y_0 - y_1) + \dot{y}_{12}(y_1 - y_2) + \dot{y}_{20}(y_2 - y_0) - [\dot{x}_{01}(x_0 - x_1) + \dot{x}_{12}(x_1 - x_2) + \dot{x}_{20}(x_2 - x_0)]\},$$

where

$$\dot{x}_{01} = \tfrac{1}{2}(\dot{x}_0 + \dot{x}_1), \text{ etc.,}$$

and

$$A = \text{area of triangle } (0, 1, 2)$$
$$= \tfrac{1}{2}[x_1(y_2 - y_0) + x_2(y_0 - y_1) + x_0(y_1 - y_2)].$$

A triangle q for zones ②, ③, and ④ is formulated in the same manner. The components of the viscosity are added to the corresponding stress in the equations of motion for point (j, k). As can be seen, the q has been formulated for plane geometry. The same q is used for cylindrical symmetry.

APPENDIX B: Tensor Artificial Viscosity for Stabilizing a Three-Dimensional Grid

For quasi-static problems in solid mechanics, nonphysical numerical oscillations can occur in the grid under certain boundary conditions. A tensor viscosity based on the rate of strain of volume elements formed by the zone corners is used to damp this type of oscillation. Referring to Fig. B.1, it is seen that surrounding point 0 there are eight tetrahedrons defined by the corners of the eight zones. A Navier–Stoke–type tensor viscosity based on the rates of strain of the tetrahedron volumes is calculated for each tetrahedron that contains point 0.

The tetrahedron corresponding to zone ① is shown in Fig. B.2, where grid point 1 corresponds to point 0 of Fig. B.1. For calculating the components of viscosity for the tetrahedron in zone ①, the finite-difference–integration–mapping procedure is applied to the four surfaces of the tetrahedron formed by vectors **A**, **B**, and **C**, of Fig. B.2.

Volume $\nu_{\mathbf{ABC}}$ formed by these vectors is given by

$$(\nu_{\mathbf{ABC}})^{n+1} = 1/6(\mathbf{B} \times \mathbf{A}) \cdot \mathbf{C} = 1/6[b_i(a_j c_k - a_k c_j) - b_j(a_i c_k - a_k c_i) + b_k(a_i c_j - a_j c_i]^{n+1}.$$

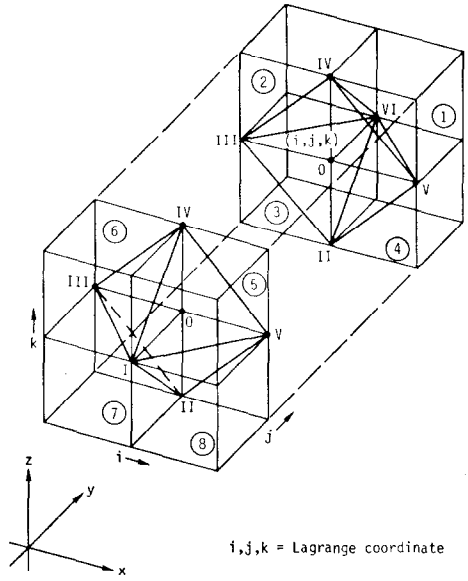

FIG. B.1. Three-dimensional grid for accelerating point (i, j, k).

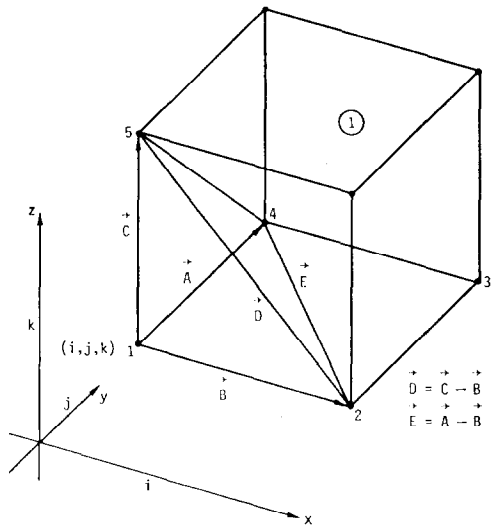

FIG. B.2. Grid numbering scheme for calculating the tensor viscosity of the tetrahedron associated with point (i, j, k) of Zone 1.

The notation for the vector components is

$$\mathbf{A}: \quad (a_i) = x_4 - x_1\,; \quad (a_j) = y_4 - y_1\,; \quad (a_k) = z_4 - z_1\,.$$

$$\mathbf{B}: \quad (b_i) = x_2 - x_1\,; \quad (b_j) = y_2 - {}_1\,; \quad (b_k) = z_2 - z_1\,.$$

$$\mathbf{C}: \quad (c_i) = x_5 - x_1\,; \quad (c_j) = y_5 - {}_1\,; \quad (c_k) = z_5 - z_1\,.$$

Velocity derivatives corresponding to the tetrahedron (Fig. B.2) are given by

$$\left(\frac{\partial \dot{x}}{\partial x}\right)^{n+1/2} = \left(\frac{1}{6\nu_{ABC}^{n+1/2}}\right)[\dot{x}_{AB}(\mathbf{A} \times \mathbf{B}) \cdot \mathbf{i} + \dot{x}_{CA}(\mathbf{C} \times \mathbf{A}) \cdot \mathbf{i} + \dot{x}_{BC}(\mathbf{B} \times \mathbf{C}) \cdot \mathbf{i} + \dot{x}_{ED}(\mathbf{E} \times \mathbf{D}) \cdot \mathbf{i}]^{n+1/2}$$

where

$$\dot{x}_{AB} = (\dot{x}_1 + \dot{x}_2 + \dot{x}_4),$$
$$\dot{x}_{CA} = (\dot{x}_1 + \dot{x}_4 + \dot{x}_5),$$
$$\dot{x}_{BC} = (\dot{x}_1 + \dot{x}_2 + \dot{x}_5),$$
$$\dot{x}_{ED} = (\dot{x}_2 + \dot{x}_4 + \dot{x}_5),$$

and

$$\nu_{ABC}^{n+1/2} = \tfrac{1}{2}[\nu_{ABC}^{n} + \nu_{ABC}^{n+1}].$$

This expression can be simplified by expressing vectors **D** and **E** in terms of vectors **A** and **B**:

$$\left(\frac{\partial \dot{x}}{\partial x}\right)^{n+1/2} = \left(\frac{1}{6\nu_{ABC}^{n+1/2}}\right)[(\dot{x}_1 - \dot{x}_5)(\mathbf{A} \times \mathbf{B}) \cdot \mathbf{i} + (\dot{x}_1 - \dot{x}_2)(\mathbf{C} \times \mathbf{A}) \cdot \mathbf{i} + (\dot{x}_1 - \dot{x}_4)(\mathbf{B} \times \mathbf{C}) \cdot \mathbf{i}]^{n+1/2},$$

where

$$(\mathbf{A} \times \mathbf{B}) \cdot \mathbf{i} = (a_j b_k - a_k b_j),$$
$$(\mathbf{C} \times \mathbf{A}) \cdot \mathbf{i} = (c_j a_k - c_k a_j),$$

and

$$(\mathbf{B} \times \mathbf{C}) \cdot \mathbf{i} = (b_j c_k - b_k c_j),$$

$$\left(\frac{\partial \dot{x}}{\partial y}\right)^{n+1/2} = \left(\frac{1}{6\nu_{ABC}^{n+1/2}}\right)[(\dot{x}_1 - \dot{x}_5)(\mathbf{A} \times \mathbf{B}) \cdot \mathbf{j} + (\dot{x}_1 - \dot{x}_2)(\mathbf{C} \times \mathbf{A}) \cdot \mathbf{j} + (\dot{x}_1 - \dot{x}_4)(\mathbf{B} \times \mathbf{C}) \cdot \mathbf{j}]^{n+1/2},$$

where

$$(\mathbf{A} \times \mathbf{B}) \cdot \mathbf{j} = -(a_i b_k - a_k b_i),$$
$$(\mathbf{C} \times \mathbf{A}) \cdot \mathbf{j} = -(c_i a_k - c_k a_i),$$

and

$$(\mathbf{B} \times \mathbf{C}) \cdot \mathbf{j} = -(b_i c_k - b_k c_i).$$

$$\left(\frac{\partial \dot{x}}{\partial z}\right)^{n+1/2} = \left(\frac{1}{6\nu_{ABC}^{n+1/2}}\right)[(\dot{x}_1 - \dot{x}_5)(\mathbf{A} \times \mathbf{B}) \cdot \mathbf{k} + (\dot{x}_1 - \dot{x}_2)(\mathbf{C} \times \mathbf{A}) \cdot \mathbf{k} + (\dot{x}_1 - \dot{x}_4)(\mathbf{B} \times \mathbf{C}) \cdot \mathbf{k}]^{n+1/2},$$

where

$$(\mathbf{A} \times \mathbf{B}) \cdot \mathbf{k} = (a_i b_j - a_j b_i),$$
$$(\mathbf{C} \times \mathbf{A}) \cdot \mathbf{k} = (c_i a_j - c_j a_i),$$

and

$$(\mathbf{B} \times \mathbf{C}) \cdot \mathbf{k} = (b_i c_j - b_j c_i).$$

To calculate:

$\frac{\partial \dot{y}}{\partial x}$ and $\frac{\partial \dot{z}}{\partial x}$, do in same way as $\frac{\partial \dot{x}}{\partial x}$ but replace $\dot{x}$ by $\dot{y}$ or $\dot{z}$;

$\frac{\partial \dot{y}}{\partial y}$ and $\frac{\partial \dot{z}}{\partial y}$, do in same way as $\frac{\partial \dot{x}}{\partial y}$ but replace $\dot{x}$ by $\dot{y}$ or $\dot{z}$;

$\frac{\partial \dot{y}}{\partial z}$ and $\frac{\partial \dot{z}}{\partial z}$, do in the same way as $\frac{\partial \dot{x}}{\partial z}$ but replace $\dot{x}$ by $\dot{y}$ or $\dot{z}$.

Components of the rate of strain of the tetrahedron defined by vectors **A**, **B**, and **C** (Fig. B.2) are

$$\dot{\epsilon}_{xx} = \frac{\partial \dot{x}}{\partial x},$$

$$\dot{\epsilon}_{yy} = \frac{\partial \dot{y}}{\partial y},$$

$$\dot{\epsilon}_{zz} = \frac{\partial \dot{z}}{\partial z},$$

$$\dot{\epsilon}_{xy} = \left[\frac{\partial \dot{x}}{\partial y} + \frac{\partial \dot{y}}{\partial x}\right],$$

$$\dot{\epsilon}_{yz} = \left[\frac{\partial \dot{y}}{\partial z} + \frac{\partial \dot{z}}{\partial y}\right],$$

$$\dot{\epsilon}_{zx} = \left[\frac{\partial \dot{x}}{\partial z} + \frac{\partial \dot{z}}{\partial x}\right],$$

and

$$\frac{\dot{v}}{v} = \frac{\partial \dot{x}}{\partial x} + \frac{\partial \dot{y}}{\partial y} + \frac{\partial \dot{z}}{\partial z}.$$

Tensor artificial viscosity for tetrahedron A, B, C (Fig. B.2) is

$$q_{xx}^{n+1/2} = 2\mu_1 \left[\dot{\epsilon}_{xx} - \frac{1}{3}\frac{\dot{v}}{v}\right]^{n+1/2},$$

$$q_{yy}^{n+1/2} = 2\mu_1 \left[\dot{\epsilon}_{yy} - \frac{1}{3}\frac{\dot{v}}{v}\right]^{n+1/2},$$

$$q_{zz}^{n+1/2} = 2\mu_1 \left[\dot{\epsilon}_{zz} - \frac{1}{3}\frac{\dot{v}}{v}\right]^{n+1/2},$$

$$q_{xy}^{n+1/2} = \mu_1[\dot{\epsilon}_{xy}]^{n+1/2},$$

$$q_{yz}^{n+1/2} = \mu_1[\dot{\epsilon}_{yz}]^{n+1/2},$$

and

$$q_{zx}^{n+1/2} = \mu_1[\dot{\epsilon}_{zx}]^{n+1/2},$$

where

$$\mu_1 = [C_{\text{NS}}(\rho^0/V)\nu_{\text{ABC}}^{1/3}]^{n+1},$$

$$C_{\text{NS}} = \text{constant} \approx 10^{-2},$$

$$\rho^0 = \text{reference density of zone } ①,$$

and

$$V = \text{relative volume of zone } ①.$$

The above components of the tensor artificial viscosity are added to the corresponding six components of the stress tensor defined at time $n + 1$. Zones 2 to 8 are treated in a similar manner; see Fig. B.1.

REFERENCES

1. J. VON NEUMANN AND R. D. RICHTMYER, *J. Appl. Phys.* **21** (1950), 232.
2. P. J. ROACHE, "Computational Fluid Dynamics," p. 232, Hermosa Publishers, Albuquerque N. M., 1972.
3. R. LANDSHOFF, "A Numerical Method for Treating Fluid Flow in the Presence of Shocks," Los Alamos Scientific Laboratory Report LA-1930, 1955.
4. V. F. KUROPATENKO, *in* "Difference Methods for Solutions of Problems of Mathematical Physics, I" (N. N. Janenko, Ed.), p. 116, Amer. Math. Soc., Providence, R. I., 1967.
5. V. F. KUROPATENKO, *Chislennye Metody Mekh. Sploshnoi Sredy* **1** (1970), 69 (AN SSSR, Novosibirsk).
6. B. L. ROZHDESTVENSKII AND N. N. JANENKO, "Sistemy kvazilineinykh uravnenii i ikh prilozheniya k gazovoi dinamike," pp. 407–435, Moscow, 1968.
7. H. HUGONIOT, *J. École Polytech.* **58** (1889), 106.
8. M. L. WILKINS, "Shock Hydrodynamics," Lawrence Livermore Laboratory Report UCRL-6797, 1962.
9. M. L. WILKINS, *in* "Methods in Computational Physics" (B. Alder, S. Fernbach, and M. Rotenberg, Eds.), Vol. 3, pp. 211–263, Academic Press, New York, 1964; also Lawrence Livermore Laboratory Report UCRL-7322 Rev. 1, 1969.
10. H. F. COOPER, JR., "Generation of an Elastic Wave by Quasi-static Isentropic Expansion of a Gas in a Spherical Cavity: Comparison between Finite Difference Predictions and the Exact Solution," pp. 2–6, Air Force Weapons Laboratory, Kirtland AFB, Albuquerque, N. M., Report AFWL-TR-66-83, 1966.
11. G. T. RICHARDS, "Derivation of a Generalized Von Neumann Pseudo-viscosity with Directional Properties," Lawrence Livermore Laboratory Report UCRL-14244, 1965.

12. A. C. ERINGEN, "Nonlinear Theory of Continuous Media," McGraw–Hill, New York, 1962.
13. P. L. PROCUNIER AND K. R. WALLACH, "Reduction of Mesh Tangling in Two-dimensional Lagrangian Hydrodynamic Codes by the Use of Viscosity, Artificial Viscosity, and TTS (Temporary Triangular Subzoning for Long, Thin Zones)," Los Alamos Scientific Laboratory Report LA-4740 MS, 1971.
14. G. MAENCHEN AND S. SACK, *in* "Methods in Computational Physics," Vol. 3, pp. 202–204, Academic Press, New York, 1964.
15. M. L. WILKINS, R. E. BLUM, E. CRONSHAGEN, AND P. GRANTHAM, "A Method for Computer Simulation of Problems in Solid Mechanics and Gas Dynamics in Three Dimensions and Time," Lawrence Livermore Laboratory Report UCRL-51574, Rev. 1, 1975.